ADVANCED MATERIALS
www.advmat.de

Stretchable Device for Simultaneous Measurements of Contractility and Electrophysiology of Neuromuscular Tissue in the Gastrointestinal Tract

Poppy Oldroyd, Sophie Oldroyd, Michelle Meng, Rajesh Makwana, Gareth Sanger, David Bulmer, George G Malliaras, and Róisín M Owens**

Devices interfacing with biological tissues can provide valuable insights into function, disease, and metabolism through electrical and mechanical signals. However, certain neuromuscular tissues, like those in the gastrointestinal tract, undergo significant strains of up to 40%. Conventional inextensible devices cannot capture the dynamic responses in these tissues. This study introduces electrodes made from poly(3,4-ethylenedioxythiophene):poly (styrenesulfonate) (PEDOT:PSS) and polydimethylsiloxane (PDMS) that enable simultaneous monitoring of electrical and mechanical responses of gut tissue. The soft PDMS layers conform to tissue surfaces during gastrointestinal movement. Dopants, including Capstone FS-30 and polyethylene glycol, are explored to enhance the conductivity, electrical sensitivity to strain, and stability of the PEDOT:PSS. The devices are fabricated using shadow masks and solution-processing techniques, providing a faster and simpler process than traditional clean-room-based lithography. Tested on ex vivo mouse colon and human stomach, the device recorded voltage changes of up to 300 µV during contraction and distension consistent with muscle activity, while simultaneously recording resistance changes of up to 150% due to mechanical strain. These devices detect and respond to chemical stimulants and blockers, and can induce contractions through electrical stimulation. They hold great potential for studying and treating complex disorders like irritable bowel syndrome and gastroparesis.

1. Introduction

The simultaneous monitoring of electrical and mechanical activity of gastrointestinal (GI) tissue is gaining significant interest due to increased understanding of the gut–brain axis.[1,2] Correlating the relationship between electrophysiological and mechanical responses within the GI tract is crucial to understanding gut physiology, and how this is altered by disease pathology, against which more stratified treatment approaches can then be directed. For example, the monitoring of gastric dysmotility as an early symptom of Parkinson's disease may facilitate the detection and early treatment of disease many years before the clinical manifestation of neurological symptoms.[3] Simultaneous monitoring of gut motility and permeability in multi-factorial functional GI disorders such as irritable bowel syndrome (IBS)[4-6] will enable changes in gut function to be considered alongside a disturbed microbiome–gut–brain axis,[7] and psychiatric comorbidities such as anxiety and depression, which are higher in

P. Oldroyd, G. G Malliaras
Electrical Engineering Division
Department of Engineering
University of Cambridge
Cambridge CB3 0FA, UK
E-mail: gm603@cam.ac.uk

S. Oldroyd, R. M Owens
Department of Chemical Engineering and Biotechnology
University of Cambridge
Cambridge CB3 0AS, UK
E-mail: rmo37@cam.ac.uk

M. Meng, D. Bulmer
Department of Pharmacology
Tennis Ct Rd
University of Cambridge
Cambridge CB2 1PD, UK

R. Makwana, G. Sanger
Blizard Institute
Queen Mary University of London
Cambridge E1 2AT, UK

The ORCID identification number(s) for the author(s) of this article can be found under https://doi.org/10.1002/adma.202312735

DOI: 10.1002/adma.202312735

some IBS subtypes.[8] In addition, localized measurement of electrophysiological and mechanical activity from areas such as the stomach in patients with gastroparesis, a neuromuscular dysfunction disorder common in diabetics, leads to delayed gastric emptying, due to altered expression of contractile proteins in smooth muscle cells,[9] and damage of the gut's pacemaker cells (Interstitial cells of Cajal).[10]

By exploring the relationships between different bio-signals and other physiological parameters, valuable insights into the origins of diseases can be gained. Organic electronics have found extensive application in the monitoring of various bio-signals and biomarkers within the human body. These applications range from cortical microelectrodes capable of recording single neurons from the surface of the brain[11] to electrochemical measurement of antibody levels for drug management.[12] However, existing devices that capture both mechanical and electrical signals rely on separate strain gauges and electrodes, thus limiting their capability to establish location-specific correlations between these signals.[13,14] To overcome this limitation, we have developed a novel device that utilizes a strain gauge for mechanical monitoring, that can also function as an electrode for electrical monitoring. This enables bimodal recording of electrical and mechanical data while maintaining location-specificity.

Organic electronic devices implemented in the gut have received relatively limited research attention despite the gut containing only 100 times fewer neurons than the brain.[15,16] This is partly because conventional stiff, or strain invariant, systems, developed primarily as neural probes, are unable to interface with the gut's dynamic surface, which can experience strain levels of up to 40%.[15] The ideal mechanical and electrical bimodal recording system should possess flexibility, softness, and a low Young's modulus to conform to the tissue, maintain high signal-to-noise ratios, and allow unrestricted tissue motion. Thin film electrodes are a promising alternative to stiff probes, as they provide good electrical contact and conform to the tissue surface without penetrating, thereby reducing scar formation, local inflammation, and glial response.[17] To fabricate thin-film electrodes, layers of substrate, conductive material, and insulation are required. Traditionally, noble metals like gold have been used for the conductive layer. However, their higher Young's modulus compared to tissue and other layers can result in buckling, delamination, and cracking.[18,19] A promising alternative is the conducting polymer poly(3,4-ethylenedioxythiophene):poly(styrenesulfonate) (PEDOT:PSS), which demonstrates long-term stability and outperforms metal electrodes that crack and degrade over time.[20] PEDOT:PSS electrodes exhibit low impedance and high charge injection capacities, indicating their effectiveness.[21] As a substrate and insulation material, polydimethylsiloxane (PDMS) shows great promise due to its superior intrinsic strain properties surpassing current polymers like polyimide and parylene C.[22,23] With a Young's modulus ranging from 0.57 to 3.7 MPa, PDMS is ideal for interfacing with GI tissue, which has a Young's modulus of 2.63 MPa in humans, when measured on intact tissue using a tensile tester.[24,25] PDMS is commonly used as a substrate in stretchable electronics, which are loosely defined as withstanding strains of over 10%.[26] Although PDMS is hydrophobic, the use of additives and surface treatments enables the enhanced adhesion of aqueous PEDOT:PSS onto PDMS.[27] By incorporating a fluorosurfactant and a hydrophilic polymer into the PEDOT:PSS solution, we achieve a solution processible and stable coating on PDMS.

By combining the aforementioned material choices and fabrication techniques with our innovative strain gauge and electrode system, we introduce a novel device fabricated with a PDMS substrate, PEDOT:PSS conducting tracts, and a PDMS insulating layer (PDMS-PEDOT:PSS-PDMS). Table S1 (Supporting Information) outlines the performance characteristics of alternative sensors employing a PEDOT:PSS and PDMS architecture. Our device proposes a distinctive composition of PEDOT:PSS that ensures sustained high conductivity for electrical recording. The device detects mechanically induced alterations in resistance, even under strains exceeding 70%—a threshold well beyond the anticipated strains within the gastrointestinal tract. Additional merits of our device encompass a consistent electrical response following 1000 stretching cycles to 40%, along with its notable thin profile, a critical factor for seamless integration with constantly moving tissues.

The device is capable of simultaneous monitoring of mechanical and electrical activity in tissues, undergoing substantial conformational changes, associated with rhymical forced distension in the gut. In contrast to traditional flexible electronic devices that depend on lengthy and expensive lithography techniques, our streamlined approach requires only four fabrication steps, all of which can be carried out outside the cleanroom environment. This significantly boosts throughput and efficiency. Utilizing the PDMS-PEDOT:PSS-PDMS devices, we demonstrate the ability to monitor ex vivo GI tract strains of up to approximately 50% while simultaneously recording real-time electrophysiology in both mouse and human tissue. This integrated approach presents a valuable tool for dual monitoring, offering insights into various diseases, diagnostics, and potential treatments based on the observed mechanical and electrical behaviors.

2. Device Fabrication and Optimization

Electrodes were fabricated using conventional spin coating techniques on top of 1″× 3″ inch glass slides. Two micrometers of parylene C was deposited as a release layer to allow for peeling off the PDMS devices. The devices were fabricated using two ≈20 µm layers of PDMS as the substrate and insulation layer, with a resultant thickness of ≈40 µm. Different thicknesses (1–100 µm) of PDMS were investigated. The handleability of the different thicknesses, as well as the spin coating parameters needed to achieve them, are shown in Table S2 (Supporting Information). The PDMS became difficult to handle at thicknesses <20 µm. Forty micrometers was chosen for tissue interfacing ex vivo applications due to the device's robust nature. However, for in vivo applications we suggest a thickness of 20 µm, combining two 10 µm layers, a recommendation based on consultation from experts in animal surgery who found this thickness optimal for manipulating in tight spaces. The mechanical properties of the PDMS can also be tuned by altering the curing time and temperature.[25] Here, we propose a 10:1 ratio of PDMS to curing agent, with curing overnight at room temperature followed by a one-hour cure at 70 °C. Such a curing protocol maintains the low Young's modulus and elongation properties of the PDMS while allowing it to be handled.

Macro-scale conductive PEDOT:PSS tracks were deposited using a laser cut shadow mask between the PDMS insulation layers (Figure S1, Supporting Information). Using a laser-cut shadow mask removes the need for traditional clean-room-based lithography to pattern the electrodes resulting in a much quicker fabrication process. The resolution, however, is limited by the diameter of the laser, which is around 100 µm. To enhance the compatibility of hydrophobic PDMS with PEDOT:PSS, the wettability of PEDOT:PSS can be improved by adding Capstone FS-30, a fluorosurfactant previously known as Zonyl.[28,29] Increasing the Capstone FS-30 weight percentage from 0.1% to 1% decreases the advancing contact drop angle from 86% to 55%, as shown in **Figure 1**A. Alternatively, the PDMS can be treated with oxygen plasma prior to the PEDOT:PSS deposition.[30] For 1 wt% Capstone FS-30, this treatment has a large effect on the advancing angle decreasing it from 55.2% to 9.3% by promoting the formation of a uniform aqueous film of PEDOT:PSS through the introduction of polar silanol groups on PDMS (Figure 1A). The initial and advancing drop angle of oxygen plasma-treated samples (Figure 1Bi) is much lower than the non-oxygen plasma-treated samples (Figure 1Bii) and enables the deposition of a homogenous film.

To evaluate the stability of the device, we used a previously published accelerated aging system.[31] The system involved placing the devices in sealed beakers containing 3% hydrogen peroxide in PBS, followed by shaking, heating, and current-controlled biphasic pulse stimulation. Figure 1C illustrates that the devices with 0.1 wt% Capstone FS-30 were unstable in solution for prolonged periods, with only 25% of the devices remaining functional after 300 days of accelerated aging. Non-functional electrodes were classified as those having two orders of magnitude changes at 1 kHz in the electrochemical impedance spectroscopy (EIS). The hydrophilic and glassy layer of SiOx that is formed upon oxygen plasma treatment, has been shown to be unstable due to the presence of crack formation which leads to electrode failure.[32] Raising the Capstone FS-30 concentration to 1 wt% resulted in a higher chronic wettability of the device, leading to over 91% of functional devices. This is likely due to the plasticizing of the PEDOT:PSS reducing brittleness.[28]

4-Point probe conductivity measurements show that for high Capstone FS-30 concentrations (10 wt%), the conductivity of the solution decreases by fourfold because the insulating Capstone FS-30 dilutes the conducting PEDOT:PSS (Figure 1D).[33] We determined that the optimal process for this application is a combination of oxygen plasma and 1 wt% Capstone, which allows for chronic stability and a high conductivity.

Pristine, free-standing PEDOT:PSS films can be stretched to between 2% and 6%, when measured using tensile testing.[34] The small strain capabilities of these films likely due to a loss of connection of the conductive PEDOT grains upon stretching. The conductivity of pristine PEDOT:PSS is dependent on a number of factors including humidity, formulation and film morphology, but varies between 0.001 and 1 S cm^{-1}.[35] Different additives such as polyethylene glycol (PEG), ethylene glycol (EG), methanol (MeOH), and dimethylsulfoxide (DMSO) have been explored to improve conductivity of PEDOT:PSS, and maintain this conductivity upon stretching.[27,36] PEG and EG are typically used as additives for improving the conductivity.[37–39] PEG was chosen for this application due to its favorable strain properties.[27] In pristine PEDOT:PSS, the PEDOT-rich cores are surrounded by PSS shells. PEG, being the polymer form of EG, interacts with PEDOT:PSS in a similar way.[37] Both lower the Coulombic interaction of the PSS chains with the PEDOT due to the formation of hydrogen bonds with the PSS. Consequently, there is an increase in PEDOT aggregation and an increase in heterogeneity of the film morphology leading to an observed increase in hole mobility enhancing the overall conductivity. Furthermore, the layers in the heterogenous structure can slide over each other, allowing maintenance of the electrical properties upon stretch.

To determine the optimal concentration of PEG, different weight percent devices were fabricated and mechanically tested until breaking. Figure 1E shows that PEDOT:PSS with 1 wt% PEG fails electrically at a very low strain of 19%. Whereas, PEDOT:PSS with 4 wt% PEG does not fail until 61% strain, greater than that needed for tissue monitoring applications. Increasing the concentration from 1 to 4 wt% has the added benefit of increasing the conductivity from 632 to 1429 S cm^{-1}, much higher than pristine PEDOT:PSS (Figure S2, Supporting Information). All formulations of Capstone FS-30 and PEG performed better in terms of strain to electrical failure than the typical microelectrode array (MEA) formulation of PEDOT:PSS (5 wt% EG, 1 wt% GOPS, 0.25 wt% DBSA).[40] Finally, 1 wt% of the crosslinker (3-Glycidyloxypropyl)trimethoxysilane (GOPS) was added to the PEDOT:PSS solution prior to spin coating.

Brightfield microscopy performed before and after stretch testing confirmed the mechanical stability of the PEDOT:PSS tracks under strain on a PDMS substrate (Figure 1F(ii–iv)). In contrast, under the same strain, PEDOT:PSS tracks deposited onto parylene C, were not stable (Figure 1F(i,ii)). The parylene-C underwent plastic deformation in the form of cracking. The images also demonstrate the high-resolution capability of the macro-fabrication method to produce PEDOT:PSS tracks with well-defined edges.

To characterize the mechanical and electrical properties of the device, a strain gauge layout was chosen for the PEDOT:PSS layer as this has proven mechanical sensitivity.[41] The electrode strain gauge design consists of a serpentine pattern that works under the principle of decreasing channel area under tension which in turn increases the resistance (**Figure 2**A). The active gauge length for the current study is 15.5 mm and the channel thickness is 1 mm, however, we note that the electrode geometry can easily be tuned for different applications, allowing the alteration of device sensitivity.

The devices should demonstrate electrical sensitivity under increasing strain, while maintaining mechanical stability and retaining these properties during cyclic testing. The mechanical properties of the device were evaluated by recording strain and force curves, while the electrical properties were characterized by recording the current across the device under a constant chronoamperometric voltage and converting it to resistance, an example curve is shown in Figure 2A. Since the device is intended for use in ex vivo and in vivo biological (aqueous) environments, properties were evaluated in an aqueous solution (setup pictured in Figure S3A,B, Supporting Information). During aqueous testing, a slight hysteresis was observed, most likely caused by the PEDOT:PSS swelling, minimized but not eliminated by the addition of GOPS, altering the properties of the electrodes. An elongation speed of either 5 mm min^{-1} for calibration or 30 mm min^{-1}

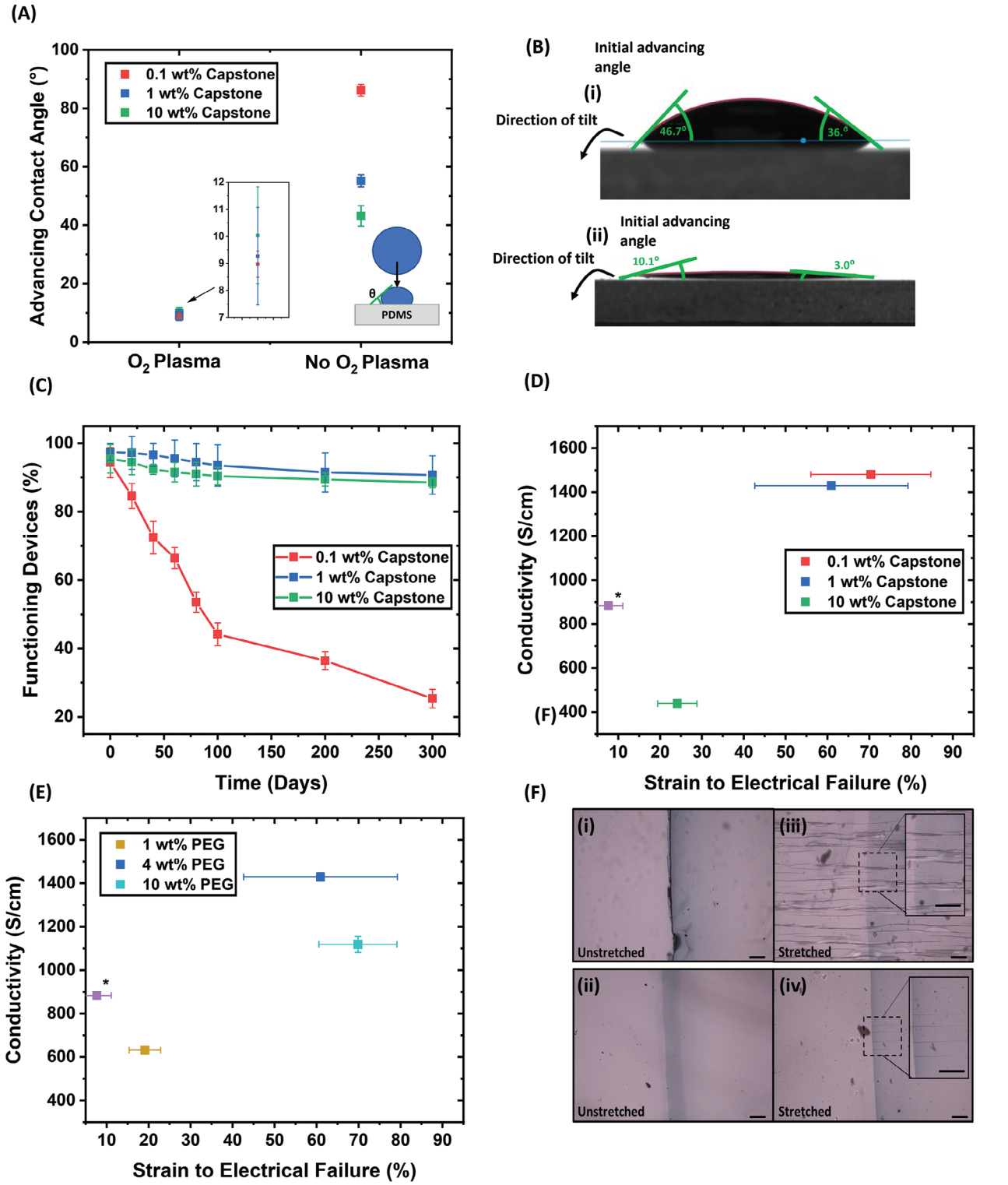

Figure 1. A) Effect of O_2 plasma and Capstone concentration on the initial angle when dropped onto PDMS. The subplot focuses on the O_2 plasma treatment. B) Representative images of initial and receding drop angles immediately after dropping 10wt% Capstone without (i) and with O_2 plasma treatment (ii) on PDMS. C) Stability of devices under accelerated aging conditions, with varying Capstone concentrations D) Comparison of initial conductivity and strain at electrical failure with varying Capstone concentrations. * (purple data point) standard MEA formulation with 5 wt% EG. E) Comparison of initial conductivity and strain at electrical failure with varying PEG concentrations. * (purple data point) standard MEA formulation with 5 wt% EG. F) Brightfield microscopy images depicting unstretched PEDOT:PSS channels on devices with PaC (i) and PDMS (ii) substrates, along with stretched channels on PaC (iii) and PDMS (iv) substrates. Stretched conditions include PaC subjected to 4 cycles at 15% strain and PDMS subjected to 1000 cycles at 40% strain, scale bar = 0.1 mm. Error bars represent mean ± standard deviation, n = 3.

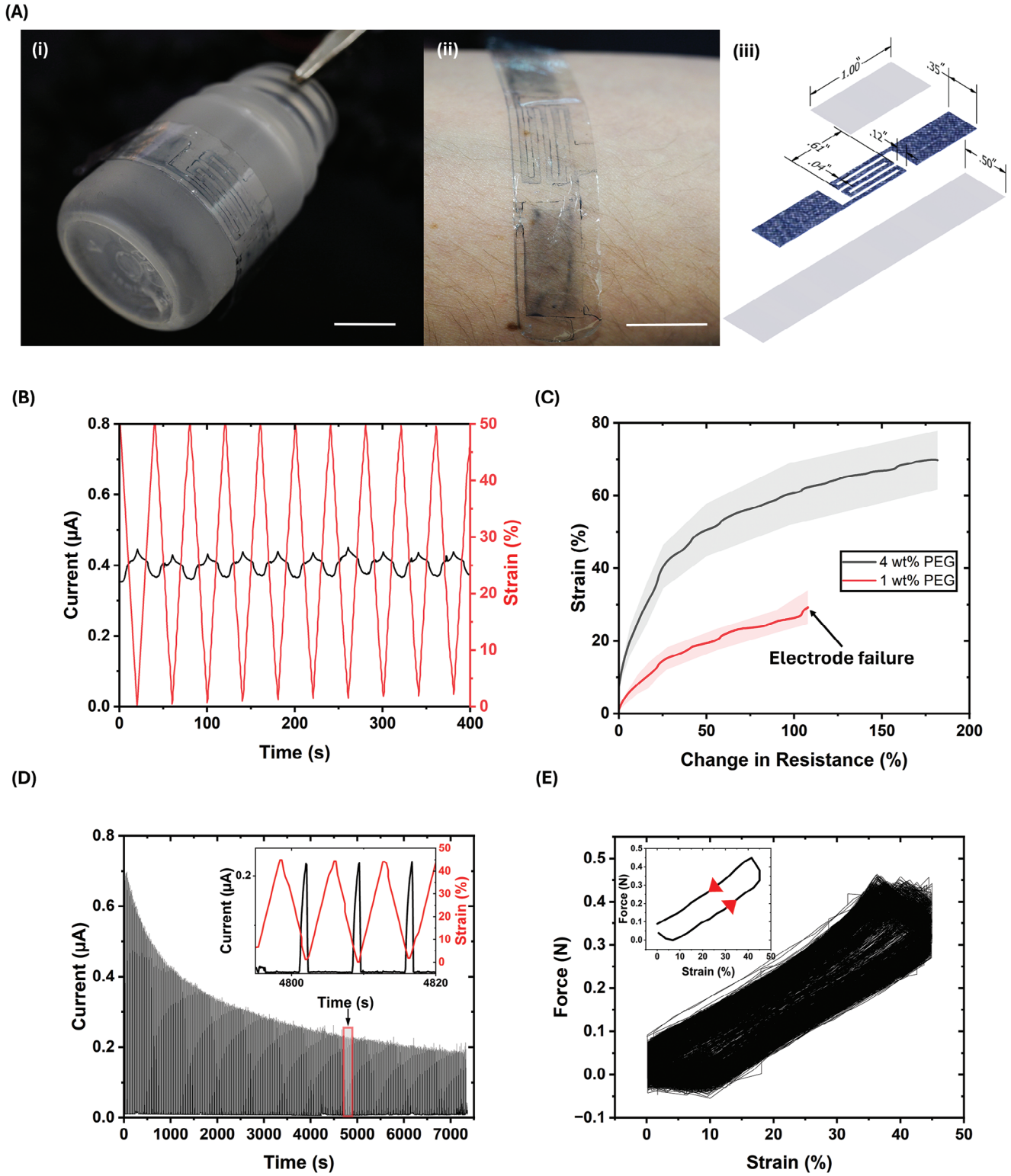

Figure 2. A, i) Image of device on plastic bottle, ii) Image of device on a forearm, iii) Schematic diagram of device, B) Cyclic testing in water, using a strain rate of 5 mm min^{-1}, C) Calibration curve correlating change in resistance with change in strain for two different PEG concentrations, shaded area represents standard deviation, n = 3. D) Cyclic testing of the 1 wt% Capstone, 4 wt% PEG device on PDMS for 1000 cycles up to 40% strain in air, using a strain rate of 30 mm/min. Subplot shows 3 cycles of testing, E) Hysteresis curves in response to the same cyclic testing. Subplot shows one hysteresis cyclic upon loading and unloading. Scale bar represents 13 mm.

for cyclic testing was used, although other elongation speeds were tested to establish that the resistance curves were not strain rate dependent (Figure S4A,B, Supporting Information).

The combination of results can be used to create a calibration curve for determining the strain for a given change in electrical resistance (Figure 2C). For 4 wt% PEG, the correlation initially displays a linear association. The gauge factor, representing the change in resistance with respect to strain, in this linear region, is ≈0.8. It plateaus at a resistance change of around 70%, corresponding to a strain of ≈60%. This indicates the dynamic range of the device. The 1 wt% PEG device is more sensitive to lower strains, with a much larger gauge factor of ≈2.5 between 0% and 20% strain. However, it fails electrically at around 30% strain. Depending on the application of the device, the appropriate concentration should be chosen; For ex vivo measurement of peristaltic activity the expected strain was ≈20%, thus 1% wt% PEG was used. A higher weight percent could be considered if the device needs to be strain insensitive to provide purely electrophysiology data. The strain sensitivity at additional PEG concentrations, and different Capstone FS-30 formulations is included in Figure S5 (Supporting Information). Capstone FS-30 has less of an effect on strain sensitivity than PEG.

The devices underwent cyclic testing to investigate their stability. Figure 2D shows the current and strain response, over 1000 cycles up to 40% strain, and the corresponding hysteresis curve is shown in Figure 2E. A slight hysteresis is observed in the current response, likely due to the small cracks observed in the PEDOT:PSS tracks (Figure 1F(iv)) after the 1000 cycles. However, the current response observed at that point is still within the detection range of the device. Cyclic testing was performed in air due to constraints with this aqueous setup. Cyclic testing was also performed on PaC devices (Figure S6A–C, Supporting Information). These devices were only able to reach strains of up to 15% because the parylene-C substrate underwent plastic deformation after each cycle resulting in irreversible and large cracks in the devices, and subsequent reduction in the electrical signal recorded. This is further seen by the cracks formed within the device shown in Figure 1F(ii).

In addition to measuring the mechanical activity, removal (or patterning) of the insulating PDMS layer allows the electrodes to be used for electrophysiological measurements. The electrode performance was validated through electrochemical impedance spectroscopy before and after cyclic testing, Figure S7A,B (Supporting Information). Electrodes before and after cyclic testing, both display a resistive regime at high frequencies and a capacitive regime at low frequencies, characteristic of PEDOT:PSS-coated thin-film electrodes.[42] Figure S7C (Supporting Information) shows the stability of the devices with minimal impedance change after cyclic stretching.

3. Monitoring Peristalsis in Ex Vivo Mouse Colon Tissue

The devices were validated in two different ex vivo setups. The first used colonic tissue from mice, while the second used human stomach tissue. A tissue bath setup was used to perform the mouse colon ex vivo experiments (**Figure** 3A,B). A 3 cm segment of mouse colon was mounted in a tissue bath using cannula tied to the tissue at oral and anal ends (Figure 3C). Tissue was perfused extraluminally (rate 7 mL min^{-1}) with warm carbogenated Krebs buffer (37 °C) to maintain tissue viability, and luminally at 0.1 mL min^{-1} with Krebs buffer to facilitate measurement of luminal pressure and distension of the intestine following temporary occlusion of the fluid outflow. Luminal pressure was repeatedly elevated and released to mimic the peristaltic action of the mouse colon.[43]

A 1 wt% PEG device was wrapped around the tissue whilst the intraluminal flow was continuous and held in place using a low viscosity silicone sealant. Resistance changes during intestinal movements were recorded using a potentiostat, and the resulting data was put through the calibration curves to translate the resistances to changes in strain (Figure 3D). The resistance/strain changes were synchronized with measurements from the internal pressure transducer, confirming the accuracy of the recorded resistance data (Figures 3D and Figure S8, Supporting Information). Slight differences were observed between the pressure and resistance peaks due to motion artefacts originating from movement of the device around the colon. Future work is being conducted on a more long-term approach to adhering the devices directly to the tissue. The response time of the device to the change in pressure was 0.89 ± 0.12 s. Forced contracted yield up to 10% strain from pressures of 8 mm Hg. To verify that the measured radial strain of the device accurately represents uniform hoop strain, mechanical testing was conducted using a balloon phantom. Hoop strain refers to the circumferential deformation or stretching experienced by the device, resembling the strain that occurs in a hoop or ring-shaped structure, like the colon, when subjected to external forces or pressure. Strain was recorded across the balloon using resistance changes with the device and dimensional changes with vernier calipers. The relationship between the two was linear, $a = 0.77b + 3.03$, where a was strain measured by the device and b was strain measured by calipers (Figure S9, Supprting Information). Although not a 1:1 relationship, the strains have less than 15% difference, likely due to non-uniform hoop strain during the initial expansion of the balloon.

In this application, the primary focus was on measuring hoop strain rather than longitudinal strain. The longitudinal sensitivity, defined as the percentage change in resistance at 40% strain, was shown to be less than 4.8% of the hoop sensitivity, meaning strain in the longitudinal direction was inconsequential (Table S3, Supporting Information). However, it is important to note that in in vivo conditions, GI propulsive movements can occur in both directions. As such, it may be beneficial in future to consider the formation of two anti-phase gauges or the utilization of a half Wheatstone bridge configuration to effectively capture the strain in these multidirectional contractions and distensions.

As previously mentioned, to achieve simultaneous electrical and mechanical recordings, the PDMS insulation layer covering the electrodes has to be removed, allowing direct contact with the outer muscularis layer of the colon. Additionally, an electrophysiological system was connected in parallel to the potentiostat, the system was grounded to the organ bath. To isolate the electrophysiology signal associated with rhymical forced distension of the bowel, the resistance change caused by the strain gauge action of the electrodes (Figure S10A, Supporting Information) and the physical stretching of the intestine were subtracted from the

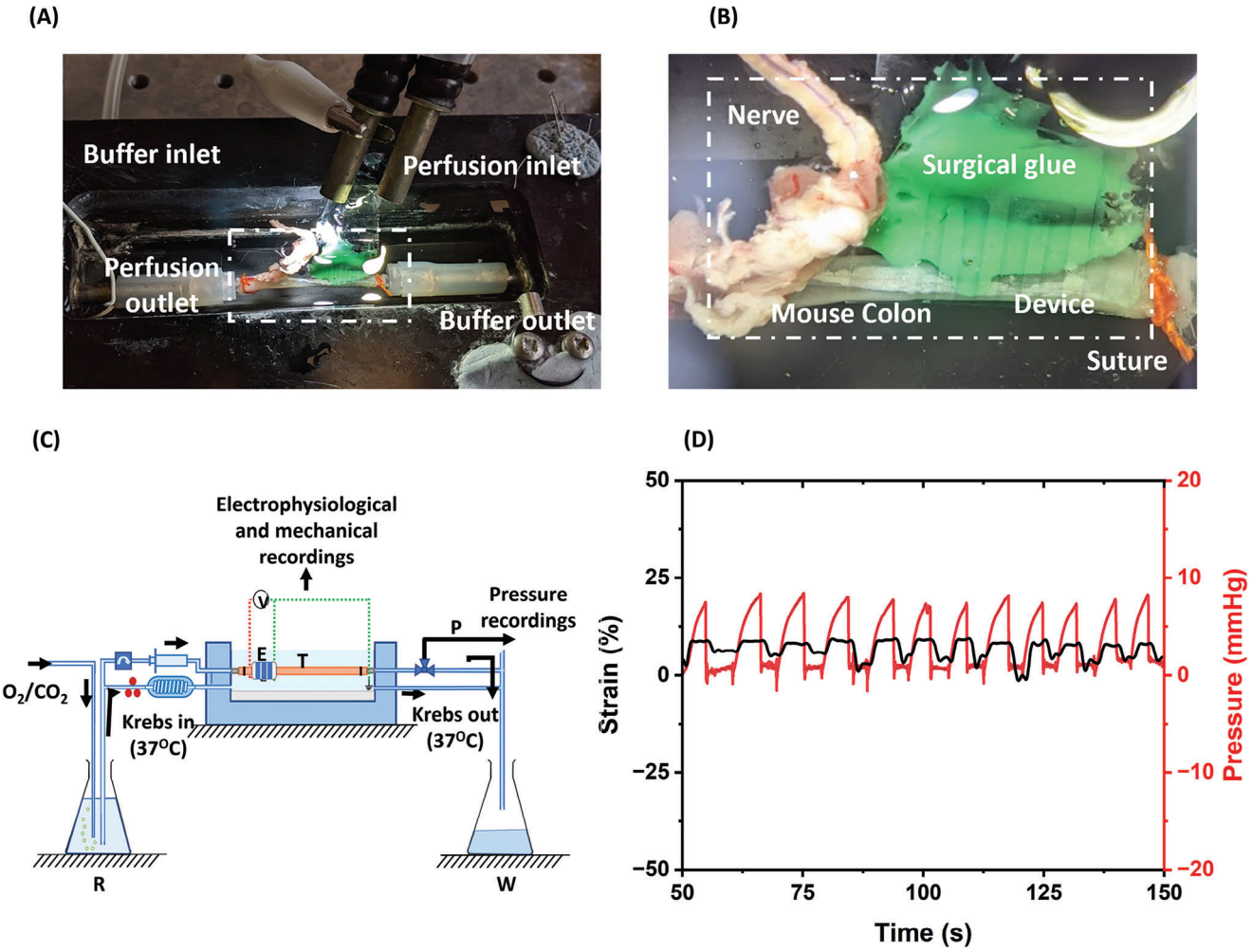

Figure 3. A,B) Optical microscopy of the device wrapped around the mouse colon secured with surgical glue and suturing to the organ bath. C) Schematic diagram of the apparatus used for simultaneous recording of smooth muscle contractions and changes in extracellular membrane potentials in mouse colon models. The recording device, E, is wrapped around the tissue which is kept viable in an organ bath. A pressure transducer, P, measures distension. Krebs buffer from the reservoir, R, is pumped into the bath via a pre-warmed heating coil. Waste Krebs is collected in a flask, W. D) Strain and pressure changes recorded during forced peristaltic action of a mouse colon.

electrophysiology data (Figure S10B, Supporting Information). The resultant waveform (Figure S10C, Supporting Information) was then processed with a notch filter at 50 Hz, a bandpass filter between 0.1 and 100 Hz, and a 50 μV amplitude filter (Figure S10D, Supporting Information).

When intestinal movements were induced, the electrophysiological voltage amplitude recorded showed an increase of 2.1–3.5 times, depending on the strength of distension (**Figure** 4A). This observed increase was found to be temporarily correlated with higher resistance levels. To validate that the signal was not a movement artefact, tissues were treated with ethanol to arrest any biological activity following which no electrophysiological responses were recorded in response to distension (Figure S10E, Supporting Information). These findings demonstrate the device's ability to successfully monitor electrical activity during distension of the intestine. Although the exact origin of this activity cannot be determined, it aligns with previous research that established a correlation between luminal pressure changes and electroenterogram data.[44]

To ensure the device was not toxic to the tissue, the device was wrapped around the colon and the nerve spike activity was recorded using a non-interfering glass suction needle electrode. Over time, the nerve activity reduces, both with and without the device, with no significant difference between the two (Figure S11A,B, Supporting Information). Furthermore, on addition of bradykinin (Bk, 1 μM), a commonly used afferent nerve stimulant,[45] the response was comparable with and without the device (Figure S11C,D, Supporting Information).

To highlight the clinical application of the devices, experiments involving chemical stimulation, blocking, and electrical stimulation were conducted. Acetylcholine (Ach) regulates gut movement,[46] and higher levels of Ach have been shown to increase motility in rat colonic tissue intestinal motility,[47] and are associated with diarrhea predominant irritable bowel syndrome

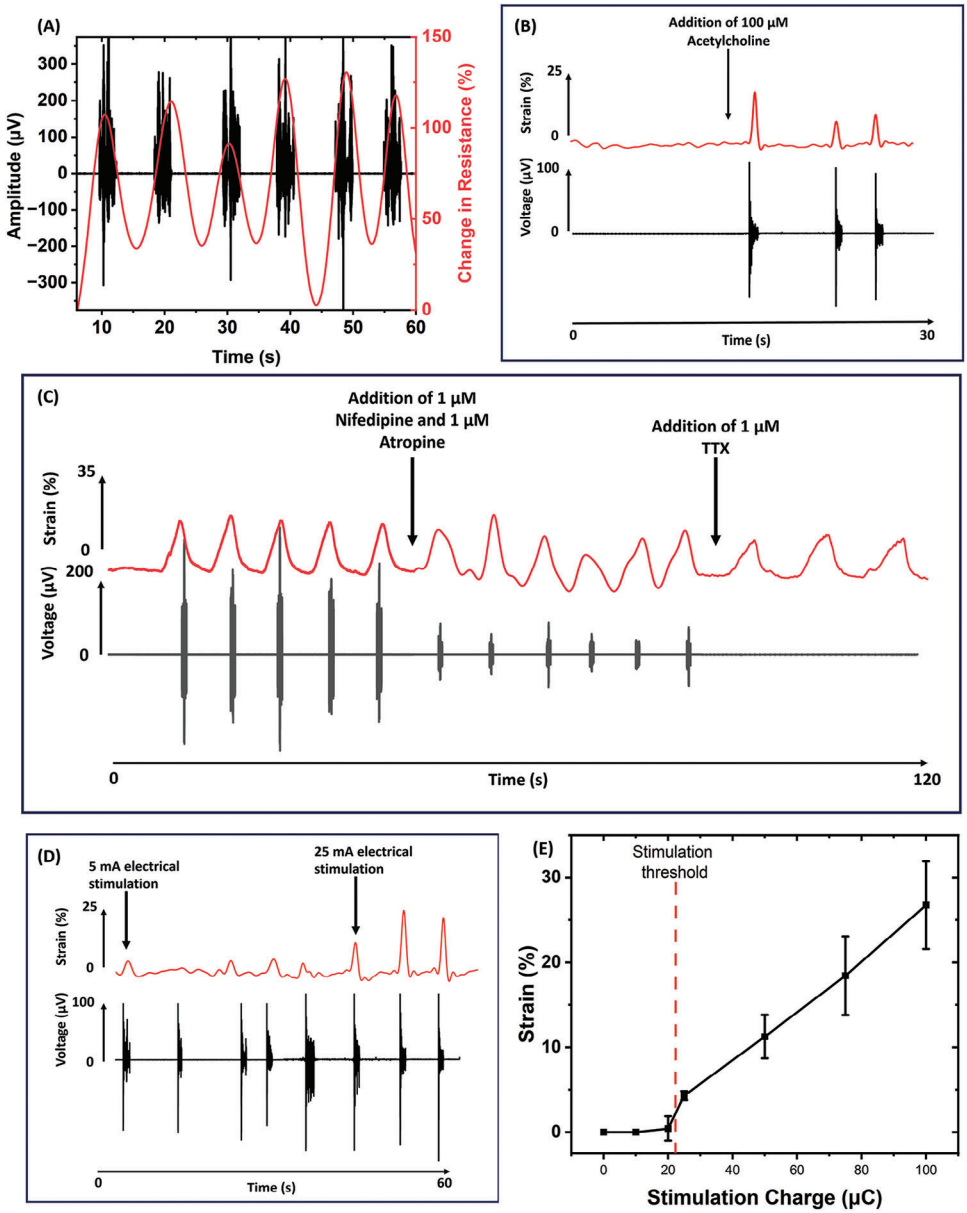

Figure 4. A) Bimodal monitoring of ex vivo mouse colon with combined mechanical and neuronal recordings upon forced peristaltic action. B) Mechanical and muscle activity recorded during the addition of the chemical stimulant acetylcholine. Spontaneous contractions observed in both strain and muscle activity. C) Mechanical and muscle activity recorded during the addition of Nifedipine and Atropine, nerve blockers, and tetrodotoxin (TTX) which is a poison that shuts down all nerve activity. Reduction and caseation of muscle activity upon forced contraction was observed. D) Simultaneous recording from and stimulation of the colon. E) Effect of stimulation charge on the strength of the triggered contraction. Stimulation threshold of 22 μC.

(IBS-D).[48] In addition, comorbidities of IBS, including anxiety and stress are associated with changes in Ach levels.[49]

The introduction of 100 μM Ach resulted in noticeable spontaneous contractions at strains up to 25%, aligning with the simultaneous recording of muscle activity by the device (Figure 4B). The device was also able to distinguish different modes of chemical blocking; Nifedipine and atropine were employed as blockers of spontaneous smooth muscle contractility, targeting the inhibition of calcium ion entry into muscle cells and blocking Ach receptors, respectively. Upon the superfusion of these chemicals under forced contractions, the electrode recorded muscle response exhibited a significant decrease of 60% (Figure 4C). Additionally, the introduction of tetrodotoxin (TTX), a poison known to inhibit voltage-gated sodium channels,[50] led to a cessation of all muscle nerve activity recordings (Figure 4C).

Furthermore, we substantiated the clinical significance of the device through the induction of contractions via electrical stimulation (Figure 4D). Individuals afflicted with IBS often grapple with impaired motility and insufficient contraction of the intestine, in the case of constipation predominant IBS (IBS-C).[51] The ability to elicit contractions within the colon presents a promising avenue for alleviating key symptoms in these patients. Notably,

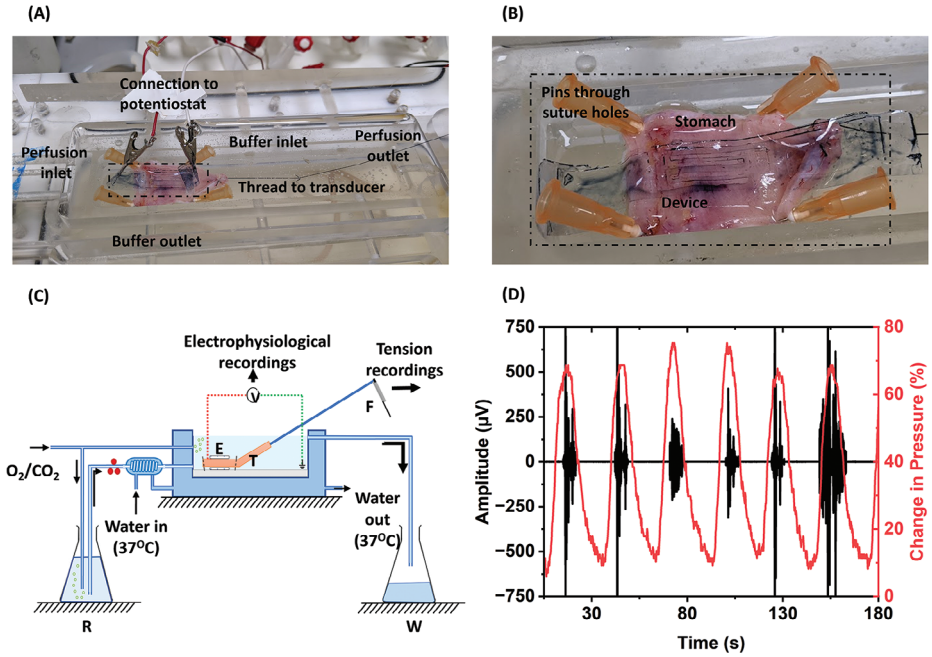

Figure 5. A,B) Experimental set-up of the device placed on top of an ex vivo stomach section. C) Schematic diagram of the apparatus used for simultaneous recording of smooth muscle contractions and changes in extracellular membrane potentials in a human stomach model. The recording device is affixed to the serosal surface of two-thirds of a muscle strip before being pinned onto the organ bath base. The free end third of the strip is attached to a force transducer, F, for measuring isometric contractions. D) Bimodal monitoring of ex vivo human stomach with combined mechanical and neuronal recordings upon isometric contraction.

upon the application of 5 mA stimulation, discernible contractions were identified in both strain and muscle activity readings obtained from the device. Importantly, as stimulation amplitude was increased above a stimulation threshold there was a linear increase in contraction force (Figure 4E).

4. Monitoring Contractions in Ex Vivo Human Stomach Tissue

The device was further validated using surgically resected human stomach tissue (**Figure** 5A). The mucosal layer of the stomach was removed by careful dissection and the tissue pinned flat allowing the device to be securely pinned flat onto the serosal surface of the stomach (Figure 5B). Upon recovery, the tissue generated spontaneous contractions that were measured using a force transducer (Figure 5C). Electrophysiological voltage changes associated with the contractions were recorded using the device (Figure 5D). Figure 4D demonstrates the peaks in voltage magnitude associated with this contractile activity. The frequency of contractions was approximately 6 per minute, slightly higher than the reported in vivo values of 3 per minute,[52] which may be related to the placement of the device. Future research will focus on investigating alternative attachment methods that are less invasive and gentler. One promising avenue is the exploration of adhesive-based approaches, which could potentially minimize tissue damage.[53]

The signals observed from the human stomach are comparable to those observed when monitoring the mouse colon, highlighting the variety of ex vivo applications of the devices and the ability to detect signals in relatively thick (human) and thin (mouse) tissues. Furthermore, the ability to wrap the electrode system around a small diameter tissue as well as affixing it to a flat surface demonstrates the flexibility of device.

The present proof-of-concept study highlights our ability to simultaneously monitor electrophysiological and contractile activity in human tissue. This has important implications for potential diagnostic uses of the device in conditions such as gastroparesis, and further experiments are now needed to confirm this utility in normal and diseased tissue in addition to other regions of the human gastrointestinal tract. Future work will include performing the chemical stimulation and blocking, and electrical stimulation experiments conducted on the mouse colon within this experimental setup.

5. Conclusion

We present a multimodal tissue monitoring device that integrates soft, flexible, and stretchable electrodes based on thin layers of PDMS and PEDOT:PSS doped with PEG and Capstone. Our simple fabrication method enables the production of highly conformable electrodes that maintain good contact with different tissues and organs, even when they undergo large contraction or distension cycles. The device's ability to detect small changes in strain and record large-scale muscle signals makes it an excellent tool for monitoring tissue health and biological activity. Moreover, its electrical sensitivity to strain can be precisely tuned for specific applications through the alteration of the various dopants in the PEDOT:PSS.

The device's flexibility and elasticity make it well-suited for monitoring gastrointestinal function, including motility and

electrical activity, as demonstrated on explanted mouse colon and human stomach tissue. Clinical relevance was demonstrated through the addition of disease-specific chemical stimulants, blockers, and through electrical stimulation-induced contractions to aid gut motility. Such a technique when used clinically, may give insight into the origin and treatment of complex disorders such as irritable bowel syndrome and gastroparesis. However, the application of this device is widespread, offering an opportunity to correlate electrophysiological activity with mechanical responses.

6. Experimental Section

Device Fabrication: Devices were fabricated using spin-coating and shadow masks. A 2 µm parylene release layer was deposited onto glass slides (1-inch x 3-inch) cleaned with acetone, isopropyl alcohol (IPA), and deionized water (Specialty Coating Systems PDS 2010 labcoater 2). PDMS was mixed in a 10:11 ratio of silicone to curing agent (SYLGARD 184), and degassed. It was then spin-coated onto the slides at 1500 rpm for 60 s and allowed to cure at room temperature overnight. A final curing at 70 °C for 1 h ensured the devices were fully cured. The devices were activated with O_2 plasma (30%) for 60 s. Shadow masks were laser-cut out of 5 µm Kapton sheets and placed onto the PDMS. For the preparation of the PEDOT:PSS, commercially available PEDOT:PSS dispersion 1 wt% (Heraeus Clevios PH1000) was used. 4 wt% Polyethylene glycol (PEG) (Sigma–Aldrich) was added to improve the electrical conductivity, 0.05% wt. dodecyl benzene sulfonic (DBSA) (Sigma–Aldrich) to improve the homogeneity of the film upon spin coating, and 1 wt% of Capstone FS-30 to promote stability and homogeneity. The mixture was then sonicated for 15 min. 1 wt% 3-Glycidyloxypropyl)trimethoxysilane (GOPS) (Sigma–Aldrich) was then added as the polymer cross-linker and the mixture was sonicated for 1 min. The solution was then passed through a 0.45 µm PTFE filter before spinning. One milliliter of PEDOT:PSS was pipetted onto the masks and spun-coat at 500 rpm for 35 s, with a subsequent soft bake at 110 °C for 60 s. The masks were removed and the PEDOT:PSS was hard baked at 110 °C for 1 h. Different solutions of 1 and 10 wt% of PEG and 0.1 and 10 wt% of Capstone FS-30 FS-30 0 were also formulated using the same method. To insulate the devices, another layer of PDMS was spin-coated at 1500 rpm for 60 s.

Mechanical and Electrical Testing: The devices were vertically loaded into a Universal Testing Machine (1ST, Tinius Olsen) with a 1 kN load cell and controlled by Horizon. They were loaded such that only the active region was stretched. A laser extensometer (500LC, Tinius Olsen) was fitted to record the strain over time. When stretching, an elongation speed of 30 mm min^{-1} was used. When performing cyclic testing a strain of 40% was always reached before reversing the direction of movement. Mechanical testing in water was performed using a custom rig (Tinius Olsen). It was not possible to use the laser with the water setup.

To couple mechanical and electrical testing, a potentiostat (Palmsens 4) was connected to each end of the device using flat crocodile clips. The potentiostat was run using chronoamperometry, with a DC voltage of 0.1 V and a time interval of 0.1 s. To record the strain to electrical failure measurements, electrical failure was taken as the point where the potentiostat records a current of less than 1 nA.

Drop Angle Measurement: Drop angle measurements were performed using a Kruss Drop Shape Analyzer DSA100. The PDMS coated glass slides were prepared as detailed above. The goniometer syringe was filled with different concentrations of PEDOT:PSS doped with capstone and PEG, a new syringe and tubing was used each time. One microliter of the sample was dispensed at a flow rate of 0.05 µL s^{-1}, so that the final drop size was 3 µL. Recording was started, and 5 µL of solution was deposited at the same flow rate. To estimate the dynamic receding and advancing angle, the sample was rotated from 0° to 90° with the rotor step sizes of 0.5 degrees per frame. The recorded images were used for analyzing the advancing and receding contact angle.

Conductivity: Conductivity measurements were performed using a custom-built 4-point probe setup. Blunt pogo-pins were inserted into a 3D printed mold, each 2 mm apart from each other. The pins were attached to a spring which applied a uniform load across the sample. 1×3″ inch glass slides were coated with the different PEDOT:PSS solutions at 500 rpm for 35 s before hard baking at 110°C for 1 hour. The thickness of each sample was recorded using a Detak profilometer.

Accelerated Aging: Devices were aged in a custom-built PTFE reaction vessel. A large Au counter electrode (CE, 2 cm × 5 cm) was patterned onto a polyimide substrate by using a polyimide shadow mask and e-beam evaporation of titanium (5 nm) and Au (100 nm). The CE was coated with the same PEDOT:PSS formulation as the electrode arrays to minimize the CE/electrolyte voltage drop. The CE was then inserted into the vessel through the lid via a hermetic insertion rubber sheet to minimize electrolyte evaporation. An Ag/AgCl electrode was used as a reference electrode (RE), this was inserted into the vessel via a tight aperture in the lid and secured with O-rings. Five milliliter of 0.01× PBS with 3% hydrogen peroxide was added to the vessel. Due to the short half-life of hydrogen peroxide, the electrolyte level was continuously monitored and replaced using a peristaltic pump system. Finally, the electrodes were connected via flat crocodile clips. The cables of which were then passed through the lid of the vessel via a hermetic insertion rubber sheet. The reaction vessel was then placed inside a Corning LSE Benchtop Shaking Incubator. For the accelerated aging, the electrodes were continuously stimulated with current-controlled biphasic pulses with an amplitude of 100 µA, a pulse width of 100 µs, an interphase gap of 33 µs, and a frequency of 200 Hz (Intan RHX Stim/Record). The shaker was set to 50 rpm and the temperature set to 70 °C.

SEM: The optical properties of the devices upon stretching and relaxing were monitored using scanning electron microscopy (Hitachi TM4000 table-top). The devices used for imaging were left without the insulation layer of PDMS, to expose the electrically conductive PEDOT:PSS. The devices were loaded onto the stage and connected using copper tape. Images were taken using 80× magnification, standard vacuum, and secondary electron detection.

Ex Vivo Application—Preparation of the Tissue: Colon tissues were obtained from male C57BL/6J mice (8-16 weeks). The mice were euthanized by cervical dislocation and exsanguination in accordance with Schedule 1 of the Animals (Scientific Procedures) Act 1986 Amendment Regulations 2012 and approval from the University of Cambridge Animal Welfare Ethical Review Body. Mice were conventionally housed in temperature-controlled rooms (21 °C) with a 12-h light/dark cycle and provided with nesting material, a red plastic shelter, and access to food and water ad libitum. Mice were primarily euthanized to obtain tissue for ongoing experiments and as such the tissue obtained for device monitoring was surplus thereby reducing animal use in line with the 3 R principles.

The intestine was stored on ice, in Krebs buffer (in M: 0.0012 $NaH_2PO_4 \cdot H_20$, 0.116 NaCl, 0.0048 KCl, 0.0012 $MgCl_2$, 0.0250 $NaHCO_3$, 0.01 D-glucose, and 1 $CaCl_2$, pre-gassed with 95% O_2/5% CO_2). A 3 cm length of the distal colon was used after trimming any fat and mesentery tissue and removal of the luminal contents by flushing with Krebs solution.

Ex Vivo Application—Organ Bath Setup: The ends of the recording device were adhered together with surgical glue (Kwik-Cast), to create a sleeve with a roughly 3 mm diameter and 1.5–2 cm length, through which a 4–5 cm length of the colon could be threaded through while still providing a close fit. This was then placed into a 50 mL rectangular organ bath (Harvard Apparatus, MA), and the tissue cannulated at either end to allow luminal perfusion with Krebs buffer using a syringe pump (Kent Scientific, 0.98 mL min^{-1} flow rate). The tissue was threaded through the device before placing in the organ bath. The tissue was also perfused serially with heated Krebs buffer (Warner in-line heater, TC-324B controller) at 37 °C using a peristaltic pump (Gilson minipuls 3) and the luminal outflow connected to a pressure transducer was connected via a T piece connector to facilitate continuous measurement of luminal pressure, captures, and digitized (100 Hz) via and A/D converter and signal processing software (Spike2, Cambridge Electronic Design). The luminal perfusion was temporally occluded to distend the bowel and trigger propulsive peristaltic movements. This allowed for the coupling of the device-based resistance

measurements with a gold standard technique. The electrical recording device was connected, via the open contact pads, to the potentiostat using flat crocodile clips, and run as previously described. This recording device was also connected to an electrophysiology module (Intan RHX Stim/Record). After setup, the tissue was left to equilibrate for a minimum of 10 min before recordings were started. The time between harvesting tissue and taking measurements was between 30 and 45 min.

For control measurements performed on fixed tissue, the intestine was initially soaked in 70% ethanol for 3 min before being sutured into the organ bath. Measurements were then taken immediately.

Ex Vivo Application—Forced Distension Measurements: Blocking the luminal outflow from the intestine, by occlusion of a three-way valve, caused the pressure to increase and the tissue to distend. These ramp manual distensions of the gut were performed so that the pressure was increased gradually for 30 s, reaching an intraluminal pressure between 8 and 15 mm Hg, before the luminal outflow was released.

Ex Vivo Application—Chemical Stimulation: For chemical stimulation, Acetylcholine chloride (Ach, 100 µM, Sigma) was added by serosal superfusion (7 mL min^{-1}) to the tissue bath (20 mL) via an in-line heater. Measurements were taken from the device 10 min after the first drug entry to the tissue bath.

Ex Vivo Application—Chemical Blocking: A baseline of muscle response was taken for forced distensions, using the method detailed above. Krebs buffer was supplemented with nifedipine (1 µmol L^{-1}) and atropine (1 µmol L^{-1}) and added by serosal superfusion. This buffer was superfused over the tissue for 10 min before forced distension measurements were taken. After this, the tissue was rinsed for 20–30 min, and the sodium channel blocker tetrodotoxin (TTX, 0.3 µmol L^{-1}) was also continuously added to the perfusing buffer in drug experiments. TTX was perfused for 10 min before repeating forced contractions to examine the muscle response.

Ex Vivo Application—Electrical Stimulation: A baseline of muscle response and strain was taken once the tissue had equilibrated. Current pulses where then delivered across the tissue to stimulate all the neurons and muscle fibers at 2 mA with charge-balanced biphasic pulses, while increasing both the pulse duration and the number of current pulses delivered (1–10 pulses). The signal was also passed through a 50 Hz notch filter to remove line noise. To determine the optimal stimulation current, a "test" stimulation was performed to initially determine if a sufficient response in the form of a contraction was achieved. To ensure the signal observed with the device, this was not a stimulation artifact, a response on the decoupled pressure sensor needed to be observed. If no response was observed, the current pulse duration and number of pulses were increased to deliver a larger charge. Stimulation was performed at three levels of distension, 0, 20, and 40 mm Hg.

Ex Vivo Electrophysiological Recording from the Lumbar Splanchnic Nerve: Following euthanasia, the colorectum with associated lumbar splanchnic nerves (LSN) were isolated. Tissue was cannulated with fine thread (Gutermann) as a tubular preparation in a recording bath with Sylgard base (Dow Corning, UK), luminally perfused (200 µL min^{-1}) by a syringe pump (Harvard Apparatus, MA) and serosally superfused (7.5 mL min^{-1}, 31–34 °C) with carbogenated (95% O_2–5% CO_2) Krebs buffer (in mM: NaCl 124, KCl 4.8, NaH_2PO_4 1.3, $CaCl_2$, $MgSO_4 \cdot H_2O$ 1.2, glucose 11.1, $NaHCO_3$ 25). Multi-unit LSN activity was recorded from teased nerve bundles using borosilicate glass suction electrodes. Signals were amplified (gain 5 kHz), bandpass filtered (100–1300 Hz; Neurolog, Digitimer Ltd, UK), and digitally filtered (Humbug, Quest Scientific, Canada) to remove 50 Hz noise. Data was digitized at 20 kHz (micro1401; Cambridge Electronic Design, UK) prior to display using Spike 2 software (Cambridge Electronic Design, UK). Action potentials were determined by counting spiking waveforms passing through a threshold set at twice the background noise (typically 10 µV).

Balloon Measurements: A tubular balloon (Azpack 178 mm, Fisher Scientific) with two open ends to allow perfusion was secured into the organ bath with the same suture techniques as the tissue, and Krebs buffer was passed luminally and serosally. The balloon was expanded using the same three-way valve as used for the experiments with the colon. The radial dimensions of the balloon were recorded before and during expansion using a digital vernier caliper. Hoop strain was calculated and compared to the calculated strain from the device.

Human Stomach Tissue Measurements: Following ethical approval (REC-15/LO/2127) and written informed consent, a resected section of human gastric antrum was obtained from an obese donor (white, male aged 45) undergoing sleeve gastrectomy as previously described.[54] This was used after overnight (≈16 h) storage at 4 °C in Krebs–Henseleit solution (×10^{-3} M: NaCl 118.3, KCl 4.7, $MgSO_4$ 1.2, KH_2PO_4 1.2, $NaHCO_3$ 25, D-glucose 11.1, $CaCl_2$ 2.5, pre-gassed with 95% O_2/5% CO_2, pH 7.4), a procedure which did not appear to affect contractile activity.[54] To prevent the release of pH-altering substances, the mucosal layer of the tissue was removed prior to overnight storage. Subsequently, two-thirds of a 5 cm × 2 cm muscle strip, cut parallel to circular muscle fibers, was securely pinned flat at the edges into a 50 mL horizontal organ bath lined with Sylgard 184 (Dow Corning, USA) with the serosal muscle surface facing upward. The tissue was bathed in oxygenated Krebs–Henseleit maintained at 37 °C and the Krebs-Henseleit solution continuously renewed at a rate of 5 mL min^{-1}. A length of cotton suture was attached to the edge of the unpinned one-third end of the muscle strip for attachment to an MLT201/D (AD Instruments, UK) force transducer for measuring isometric muscle contractions using AcqKnowledge ver3.8 (BioPAc systems, USA). The electrical recording device was pinned flat onto the serosal muscle surface and connected to the Intan system (Intan RHX Stim/Record). Following an initial manual stretch generating 20 mN, and equilibration period spontaneous contractions, caused by depolarization of the interstitial cells of Cajal, the pacemaker cells largely responsible for generating slow-wave electrical activity within the stomach were observed, and electrical recordings were started.

Data Analysis: All electrophysiology signals presented were preprocessed by applying notch filtering at 50 Hz and bandpass filtering between 0.1 and 100 Hz. Data obtained due to the change in impedance from mechanical motion was subtracted from the preprocessed electrophysiology signal. The resultant data were then amplitude filtered at 50 µV to remove baseline electrical noise.

Supporting Information

Supporting Information is available from the Wiley Online Library or from the author.

Acknowledgements

The authors would like to thank Andrew Rayment (Department of Material Science at Metallurgy, University of Cambridge) for his help in setting up the tensile testing measurements. P.O. would like to acknowledge funding from the EPRSC and Johnson Matthey iCASE studentship (G102881), and the Royal Commission of the Exhibition of 1851 (G106790). S.O. was supported by the UK Engineering and Physical Sciences Research Council (EPSRC) grant (EP/S023046/1) for the EPSRC Centre for Doctoral Training in Sensor Technologies for a Healthy and Sustainable Future. M.M. was funded by an AstraZeneca Ph.D. Studentship (G104109). This material was based upon work supported by the Air Force Office of Scientific Research under award number FA8655-20-1-7021 (for RMO). The graphical abstract was created on Biorender.com

Conflict of Interest

The authors declare no conflict of interest.

Data Availability Statement

The data that support the findings of this study are available from the corresponding author upon reasonable request.

Keywords

bioelectronics, electrodes, electrophysiology, organic, PDMS, PEDOT:PSS, stretchable

Received: November 26, 2023
Revised: January 15, 2024
Published online:

[1] J. F. Cryan, K. J. O'riordan, C. S. M. Cowan, K. V. Sandhu, T. F. S. Bastiaanssen, M. Boehme, M. G. Codagnone, S. Cussotto, C. Fulling, A. V. Golubeva, K. E. Guzzetta, M. Jaggar, C. M. Long-Smith, J. M. Lyte, J. A. Martin, A. Molinero-Perez, G. Moloney, E. Morelli, E. Morillas, R. O'connor, J. S. Cruz-Pereira, V. L. Peterson, K. Rea, N. L. Ritz, E. Sherwin, S. Spichak, E. M. Teichman, M. van de Wouw, A. P. Ventura-Silva, S. E. Wallace-Fitzsimons, et al., *Physiol. Rev.* **2019**, *99*, 1877.
[2] M. Carabotti, A. Scirocco, M. A. Maselli, C. Severi, *Ann Gastroenterol* **2015**, *28*, 203.
[3] R. A. Travagli, K. N. Browning, M. Camilleri, *Nat. Rev. Gastroenterol. Hepatol.* **2020**, *17*, 673.
[4] Q. Q. Zhou, B. Zhang, G. N. Verne, *Pain* **2009**, *146*, 41.
[5] Y. Tanaka, M. Kanazawa, S. Fukudo, D. A. Drossman, *J Neurogastroenterol Motil* **2011**, *17*, 131.
[6] J. E. Kellow, S. F. Phillips, *Gastroenterology* **1987**, *92*, 1885.
[7] P. J. Kennedy, J. F. Cryan, T. G. Dinan, G. Clarke, *World J. Gastroenterol.* **2014**, *20*, 14105.
[8] G. Fond, A. Loundou, N. Hamdani, W. Boukouaci, A. Dargel, J. Oliveira, M. Roger, R. Tamouza, M. Leboyer, L. Boyer, *Eur. Arch. Psychiatry Clin. Neurosci.* **2014**, *264*, 651.
[9] B. P. Herring, A. M. Hoggatt, A. Gupta, S. Griffith, A. Nakeeb, J. N. Choi, M. T. Idrees, T. Nowak, D. L. Morris, J. M. Wo, *Neurogastroenterol. Motil.* **2018**, *30*, 13230.
[10] C. E. Bernard, S. J. Gibbons, I. S. Mann, L. Froschauer, H. P. Parkman, S. Harbison, T. L. Abell, W. J. Snape, W. L. Hasler, R. W. McCallum, I. Sarosiek, L. A. B. Nguyen, K. L. Koch, J. Tonascia, F. A. Hamilton, M. L. Kendrick, K. R. Shen, P. J. Pasricha, G. Farrugia, *Neurogastroenterol. Motil.* **2014**, *26*, 1275.
[11] D. Khodagholy, J. N. Gelinas, T. Thesen, W. Doyle, O. Devinsky, G. G. Malliaras, G. Buzsáki, *Nat. Neurosci.* **2014**, *18*, 310.
[12] S. L. Bidinger, S. T. Keene, S. Han, K. W. Plaxco, G. G. Malliaras, T. Hasan, *Sci. Adv.* **2022**, *8*, 4111.
[13] F. Qian, C. Huang, Y. D. Lin, A. N. Ivanovskaya, T. J. O'Hara, R. H. Booth, C. J. Creek, H. A. Enright, D. A. Soscia, A. M. Belle, R. Liao, F. C. Lightstone, K. S. Kulp, E. K. Wheeler, *Lab Chip* **2017**, *17*, 1732.
[14] S. Song, F. Fallegger, A. Trouillet, K. Kim, S. P. Lacour, *Sci Robot* **2023**, *8*, eadd1002.
[15] R. G. Lentle, C. M. Hulls, *Front. Physiol.* **2018**, *9*, 338.
[16] M. Carabotti, A. Scirocco, M. A. Maselli, C. Severi, *Ann. Gastroenterol.* **2015**, *28*, 203.
[17] P. Oldroyd, G. G. Malliaras, *Acta Biomater.* **2022**, *139*, 65.
[18] P. F. Johnson, L. L. Hench, *Brain Behav. Evol.* **1977**, *14*, 23.
[19] V. I. Egorov, I. V. Schastlivtsev, E. V. Prut, A. O. Baranov, R. A. Turusov, *J. Biomech.* **2002**, *35*, 1417.
[20] C. D. Lee, E. Meng, *Front. Mech. Eng.* **2015**, *1*, 10.
[21] P. Oldroyd, J. Gurke, G. G. Malliaras, P. Oldroyd, J. Gurke, G. G. Malliaras, *Adv. Funct. Mater.* **2023**, *33*, 2208881.
[22] M. V. Hoang, H. J. Chung, A. L. Elias, *J. Micromech. Microeng.* **2016**, *26*, 105019.
[23] C. Y. Shih, T. A. Harder, Y. C. Tai, *Microsystem Technologies* **2004**, *10*, 407.
[24] H. S. Hosseini, J. C. Y. Dunn, *Bioengineering* **2020**, *7*, 1.
[25] Z. Wang, A. A. Volinsky, N. D. Gallant, *J. Appl. Polym. Sci.* **2014**, *131*.
[26] L. V. Kayser, D. J. Lipomi, *Adv. Mater.* **2019**, *31*, 1806133.
[27] M. H. Jeong, A. Sanger, S. B. Kang, Y. S. Jung, I. S. Oh, J. W. Yoo, G. H. Kim, K. J. Choi, *J Mater Chem A Mater* **2018**, *6*, 15621.
[28] S. Savagatrup, E. Chan, S. M. Renteria-Garcia, A. D. Printz, A. V. Zaretski, T. F. O'Connor, D. Rodriquez, E. Valle, D. J. Lipomi, *Adv. Funct. Mater.* **2015**, *25*, 427.
[29] M. Vosgueritchian, D. J. Lipomi, Z. Bao, *Adv. Funct. Mater.* **2012**, *22*, 421.
[30] S. H. Tan, N. T. Nguyen, Y. C. Chua, T. G. Kang, *Biomicrofluidics* **2010**, *4*, 032204.
[31] P. Oldroyd, J. Gurke, G. G. Malliaras, P. Oldroyd, J. Gurke, G. G. Malliaras, *Adv. Funct. Mater.* **2023**, *33*, 2208881.
[32] Y. Gorbanev, A. Privat-Maldonado, A. Bogaerts, *Anal. Chem.* **2018**, *90*, 13151.
[33] A. Dauzon, T. D. Citation Dauzon, E. Dauzon, Y. Lin, H. Faber, E. Yengel, X. Sallenave, C. Plesse, F. Goubard, A. Amassian, T. D. Anthopoulos, E. Dauzon, Y. Lin, H. Faber, E. Yengel, T. D. Anthopoulos, X. Sallenave, C. Plesse, F. Goubard, *Adv. Funct. Mater.* **2020**, *30*, 2001251.
[34] U. Lang, N. Naujoks, J. Dual, *Synth. Met.* **2009**, *159*, 473.
[35] H. Shi, C. Liu, Q. Jiang, J. Xu, *Adv. Electron. Mater.* **2015**, *1*, 1500017.
[36] L. W. Lo, J. Zhao, H. Wan, Y. Wang, S. Chakrabartty, C. Wang, *ACS Appl. Mater. Interfaces* **2021**, *13*, 21693.
[37] D. Alemu Mengistie, P. C. Wang, C. W. Chu, *J Mater Chem A Mater* **2013**, *1*, 9907.
[38] P. Li, K. Sun, J. Ouyang, *ACS Appl. Mater. Interfaces* **2015**, *7*, 18415.
[39] Y. Kim, C. Park, S. Im, J. H. Kim, *Sci. Rep.* *10*, 16488.
[40] D. Khodagholy, T. Doublet, M. Gurfi nkel, P. Quilichini, E. Ismailova, P. Leleux, T. Herve, S. Sanaur, C. Bernard, G. G. Malliaras, D. Khodagholy, T. Doublet, M. Gurfi nkel, E. Ismailova, P. Leleux, S. Sanaur, G. G. Malliaras, P. Quilichini, C. Bernard, T. Herve, *Adv. Mater.* **2011**, *23*, H268.
[41] U. Lang, P. Rust, J. Dual, *Microelectron. Eng.* **2008**, *85*, 1050.
[42] D. A. Koutsouras, P. Gkoupidenis, C. Stolz, V. Subramanian, G. G. Malliaras, D. C. Martin, *ChemElectroChem* **2017**, *4*, 2321.
[43] T. C. Seerden, W. J. E. P. Lammers, B. Y. De Winter, J. G. De Man, P. A. Pelckmans, *Am. J. Physiol.* **2005**, *289*, G1043.
[44] J. L. Martinez-De-Juan, J. Saiz, M. Meseguer, J. L. Ponce, *Med Eng Phys* **2000**, *22*, 189.
[45] C. McGuire, G. Boundouki, J. R. F. Hockley, D. Reed, V. Cibert-Goton, M. Peiris, V. Kung, J. Broad, Q. Aziz, C. Chan, S. Ahmed, M. A. Thaha, G. J. Sanger, L. A. Blackshaw, C. H. Knowles, D. C. Bulmer, *Gut* **2018**, *67*, 86.
[46] M. Rosas-Ballina, K. J. Tracey, *J. Intern. Med.* **2009**, *265*, 663.
[47] J. P. Russell, E. Mohammadi, C. Ligon, R. Latorre, A. C. Johnson, B. Hoang, D. Krull, M. W. Y. Ho, H. S. Eidam, M. P. DeMartino, M. Cheung, A. I. Oliff, S. Kumar, B. Greenwood-Van Meerveld, *Neurogastroenterol. Motil.* **2019**, *31*, 13479.
[48] K. Hod, A. D. Sperber, N. Maharshak, Y. Ron, I. Shapira, Z. David, O. Rogowski, S. Berliner, S. Shenhar-Tsarfaty, R. Dekel, *Neurogastroenterol. Motil.* **2018**, *30*, 13464.
[49] Y. X. Leng, Y. Y. Wei, H. Chen, S. P. Zhou, Y. L. Yang, L. P. Duan, *Chin. Med. J.* **2010**, *123*, 227.
[50] H. L. Chong, P. C. Ruben, *Channels* **2008**, *2*, 407.
[51] S. A. Peters, S. Edogawa, W. J. Sundt, R. B. Dyer, D. A. Dalenberg, A. Mazzone, R. J. Singh, N. Moses, T. C. Smyrk, C. Weber, D. R. Linden, W. K. Macnaughton, J. R. Turner, M. Camilleri, D. A. Katzka, G. Farrugia, M. Grover, *Am. J. Gastroenterol.* **2017**, *112*, 913.
[52] C. J. Stoddard, R. H. Smallwood, H. L. Duthie, *Gut* **1981**, *22*, 705.
[53] H. Yuk, C. E. Varela, C. S. Nabzdyk, X. Mao, R. F. Padera, E. T. Roche, X. Zhao, *Nature* **2019**, *575*, 169.
[54] R. Makwana, E. Crawley, M. Straface, A. Palmer, A. Gharibans, K. Devalia, J. Loy, G. O'Grady, P. L. R. Andrews, G. J. Sanger, *Br. J. Pharmacol.* **2022**, *179*, 5305.